Numerical comparison of nonlocal macroscopic models of multi-population pedestrian flows with anisotropic kernel

Paola Goatin, Daniel Inzunza, Luis Miguel Villada

Numerical comparison of nonlocal macroscopic models of multi-population pedestrian flows with anisotropic kernel

Paola Goatin, Daniel Inzunza and Luis Miguel Villada

Abstract We propose three variants of a nonlocal macroscopic pedestrian flow model accounting for anisotropic interactions between different groups and including the presence of walls or other obstacles in the walking domain. We compare the solutions behaviour in the case of bi-directional flows and othogonally crossing flows by numerical simulation based on high order finite difference schemes.

1 Introduction

Macroscopic models of (vehicular and pedestrian) traffic flow, including integral dependencies on the unknowns, have been introduced and studied in the last decade by several authors [1, 2, 4, 5, 6, 7, 11]. The nonlocal dependencies of the flux function is intended to model the agents' reaction to the presence of other agents in a (downstream) neighborhood of their location. In particular, nonlocal models allow to reproduce some characteristic behaviour of pedestrian flows, such as lane formation and other interesting patterns. Also, they can intrinsically account for the presence of obstacles in the walking domain, as explained in [3], avoiding the enforcement of an artificial vector field mimicking the discomfort close to obstacles, see e.g. [4].

In this paper, we extend the approach described in [3] to the presence of two populations with different preferred velocities (given by different targets), which interact while crossing each other on the walking domain. In particular, we propose three model variants, defined by their nonlocal dependencies, and we study the model behaviours in different situations and with different interaction parameters.

Paola Goatin and Daniel Inzunza
Université Côte d'Azur, Inria, CNRS, LJAD, Sophia Antipolis, France, e-mail: {paola.goatin,daniel-eduardo.inzunza-herrera}@inria.fr

Luis Miguel Villada
GIMNAP-Departamento de Matemáticas, Universidad del Bío-Bío, Concepción, Chile; CI^{2}MA-Universidad de Concepción, Casilla 160-C, Concepción, Chile, e-mail: lvillada@ubiobio.cl

2 Nonlocal macroscopic pedestrian flow models

We refer to the class of nonlocal crowd dynamics models for two populations with different destinations trying to avoid each other in a confined environment and described by their densities ρ^1 and ρ^2. We consider the following initial-boundary value problem for a non-local system of two conservation laws that describes the evolution of the pedestrian density $\boldsymbol{\rho} = (\rho^1, \rho^2)^T$ as a function of time t and position $\mathbf{x} = (x_1, x_2)$ on a walking domain $\Omega \subset \mathbb{R}^2$:

$$\begin{cases} \partial_t \boldsymbol{\rho} + \mathrm{div}_{\mathbf{x}} F\left(\boldsymbol{\rho}, \boldsymbol{\nu}\big(\mathbf{x}, \mathcal{I}[\boldsymbol{\rho}(t)](\mathbf{x})\big)\right) = 0, & \mathbf{x} \in \Omega, t \geq 0, \\ \boldsymbol{\rho}(0, \mathbf{x}) = \boldsymbol{\rho}_0(\mathbf{x}), & \mathbf{x} \in \Omega, \\ \boldsymbol{\rho}(t, \mathbf{x}) = 0, & \mathbf{x} \in \partial\Omega. \end{cases} \tag{1}$$

Here $\boldsymbol{\nu} = (\boldsymbol{\nu}^1, \boldsymbol{\nu}^2)^T$ with $\boldsymbol{\nu}^k = (\nu_1^k, \nu_2^k)$, $k = 1, 2$, are two vector fields that (with slight abuse of notation) are defined as

$$\boldsymbol{\nu}^k(t, \mathbf{x}) := \boldsymbol{\nu}^k\big(\mathbf{x}, \mathcal{I}_k[\boldsymbol{\rho}(t)](\mathbf{x})\big) = (1 - \epsilon_1 \mathcal{I}_k[\boldsymbol{\rho}(t)](\mathbf{x}))\boldsymbol{\mu}^k(\mathbf{x}) - \epsilon_2 \mathcal{I}_k[\nabla \boldsymbol{\rho}(t)](\mathbf{x}), \tag{2}$$

where $\boldsymbol{\mu}^k$ are the (normalized) fixed smooth vector fields of preferred directions (e.g., given by the regularized solution of an eikonal equation), and $\mathcal{I}_k[\boldsymbol{\rho}(t)]$ are non-local correction terms that depend on the current density distribution, where the notation indicates a functional dependence, i.e., $\mathcal{I}_k$ depends on the function $\boldsymbol{\rho}(t) := \boldsymbol{\rho}(t, \cdot)$ as a whole. Also, $\epsilon_1 > 0$ and $\epsilon_2 > 0$ are scaling factors, which temper the impact of the correction terms. In particular, we consider the following models:

$$\textbf{(M1)} \begin{cases} \partial_t \rho^1 + \mathrm{div}_{\mathbf{x}}\left[V_1 \rho^1 (1 - \rho^1)\left(\left(1 - \varepsilon_1 \mathcal{I}_1(\rho^1)\right)\boldsymbol{\mu}^1(\mathbf{x}) - \varepsilon_2 \mathcal{I}_1(\nabla \rho^2)\right)\right] = 0, \\ \partial_t \rho^2 + \mathrm{div}_{\mathbf{x}}\left[V_2 \rho^2 (1 - \rho^2)\left(\left(1 - \varepsilon_1 \mathcal{I}_2(\rho^2)\right)\boldsymbol{\mu}^2(\mathbf{x}) - \varepsilon_2 \mathcal{I}_2(\nabla \rho^1)\right)\right] = 0, \end{cases}$$

$$\textbf{(M2)} \begin{cases} \partial_t \rho^1 + \mathrm{div}_{\mathbf{x}}\left[V_1 \rho^1 (1 - \rho^1)\left(\left(1 - \varepsilon_1 \mathcal{I}_1(\rho^1 + \rho^2)\right)\boldsymbol{\mu}^1(\mathbf{x}) - \varepsilon_2 \mathcal{I}_1(\nabla \rho^2)\right)\right] = 0, \\ \partial_t \rho^2 + \mathrm{div}_{\mathbf{x}}\left[V_2 \rho^2 (1 - \rho^2)\left(\left(1 - \varepsilon_1 \mathcal{I}_2(\rho^1 + \rho^2)\right)\boldsymbol{\mu}^2(\mathbf{x}) - \varepsilon_2 \mathcal{I}_2(\nabla \rho^1)\right)\right] = 0, \end{cases}$$

$$\textbf{(M3)} \begin{cases} \partial_t \rho^1 + \mathrm{div}_{\mathbf{x}}\left[V_1 \rho^1 (1 - \mathcal{I}_1(\rho^1 + \rho^2))\left(\boldsymbol{\mu}^1(\mathbf{x}) - \varepsilon_2 \mathcal{I}_1(\nabla \rho^2)\right)\right] = 0, \\ \partial_t \rho^2 + \mathrm{div}_{\mathbf{x}}\left[V_2 \rho^2 (1 - \mathcal{I}_2(\rho^1 + \rho^2))\left(\boldsymbol{\mu}^2(\mathbf{x}) - \varepsilon_2 \mathcal{I}_2(\nabla \rho^1)\right)\right] = 0, \end{cases}$$

where

$$\mathcal{I}_k(\rho) := \frac{\eta_i *_w \rho}{\sqrt{1 + \|\eta_i *_w \rho\|^2}}.$$

Above, for $k = 1, 2$, η_k are smooth non-negative kernels with compact support such that $\iint_{\mathbb{R}^2} \eta_k(\mathbf{x})\, \mathrm{d}\mathbf{x} = 1$ and $V_k > 0$ are the pedestrians' maximal speeds.
Therefore, each pedestrian moves in the preferred direction $\boldsymbol{\mu}^k(\mathbf{x})$ but scales its speed according to the presence of other people (either its own population as in model (**M1**) or both population as in (**M2**) and (**M3**)), which it sees in its horizon.

The k-th population also deviates from its preferred trajectory due to the interaction with the individuals of the ℓ-th population according to $-\epsilon_2 \mathcal{I}_k(\nabla\rho^\ell)$.

To account for the presence of boundaries, in the form of walls or other obstacles, as in [3] the convolution product $*_w$ is defined as

$$\big(\eta *_w \rho(t)\big)(\mathbf{x}) = \iint_{\mathbb{R}^2} \rho_w(t,\mathbf{y})\eta(\mathbf{x}-\mathbf{y})\,\mathrm{d}\mathbf{y}, \tag{3}$$

where $\rho_w : \mathbb{R}^2 \to \mathbb{R}^+$ is the extension of the pedestrian density including the presence of obstacles:

$$\rho_w(t,\mathbf{x}) := \begin{cases} \rho(t,\mathbf{x}) & \text{if } \mathbf{x}\in\Omega, \\ R_w & \text{if } \mathbf{x}\in B(\Omega, d(\operatorname{supp}\eta))\setminus\Omega, \\ 0 & \text{elsewhere,} \end{cases} \tag{4}$$

with $R_w \geq 1$ big enough so that $\boldsymbol{\nu}(t,\mathbf{x})\cdot\mathbf{n}(\mathbf{x}) \leq 0$ for all $\mathbf{x}\in\partial\Omega$, $t\geq 0$, where $\mathbf{n}$ is the outward normal to Ω.[1]

Aiming at reproducing the limited vision field of pedestrians, oriented towards the direction of movement, we consider conic convolution kernels constructed as follows: given a kernel function $\eta(\mathbf{x})$ with compact support, we cut a conic section $\eta(\mathbf{x})\chi_{\mathcal{S}(\mathbf{x},l,\alpha,\boldsymbol{\gamma}_i)}(\mathbf{x})$ of angle 2α oriented in direction $\boldsymbol{\gamma}_k(\mathbf{x})$, $k=1,2$, which is described by the region

$$\mathcal{S}(\mathbf{x},l,\alpha,\boldsymbol{\gamma}_i) = \left\{ \mathbf{y}\in\mathbb{R}^2 : \|\mathbf{y}-\mathbf{x}\| \leq l, \frac{(\mathbf{y}-\mathbf{x})\cdot\boldsymbol{\gamma}_i(\mathbf{x})}{\|\mathbf{y}-\mathbf{x}\|\|\boldsymbol{\gamma}_i(\mathbf{x})\|} \geq \cos\alpha \right\}.$$

The section $\eta\chi_{\mathcal{S}(\mathbf{x},l,\alpha,\boldsymbol{\gamma}_i)}$ is smoothed by convolution with a Gaussian kernel $g(\mathbf{x}) = \exp(-(\|\mathbf{x}\|^2/2\sigma))$ with $\sigma = 5\times10^{-4}$, then normalized and finally shifted so that the maximum of the normalized smoothed kernel is centered in $(0,0)$, see Example 2 in [3] for more details.

3 Numerical scheme

We consider $\Omega = [a,b]\times[c,d]$ and we use a uniform Cartesian grid with nodes (x_1^i, x_2^j), $i=1,\dots,M$ and $j=1,\dots,N$ such that $x_1^i = (i-1/2)h_1, x_2^j = (j-1/2)h_2$, where $h_1 = (b-a)/M$ and $h_2 = (d-c)/N$. This provides $M\times N$ grid points $\mathbf{x}_\mathbf{i} := (x_1^i, x_2^j)$, where $\mathbf{i} = (i,j) \in \mathcal{M} := \{1,\dots,M\}\times\{1,\dots,N\}$. Moreover, the two dimensional unit vectors $\mathbf{e}_1 := (1,0)$ and $\mathbf{e}_2 := (0,1)$ allow to denote neighbouring grid points as $\mathbf{x}_{\mathbf{i}+\mathbf{e}_1} = (x_1^{i+1}, x_2^j)$ and $\mathbf{x}_{\mathbf{i}+\mathbf{e}_2} = (x_1^i, x_2^{j+1})$. As in [3], we denote by $\boldsymbol{u} : [0,+\infty) \to \mathbb{R}^{2\times M\times N}$ the solution of (1) computed at time t in the grid points

[1] We denote by $d(A) = \sup\{|\mathbf{x}-\mathbf{y}|\colon \mathbf{x},\mathbf{y}\in A\}$ the diameter of a set $A\subset\mathbb{R}^2$ and by $B(\Omega,\ell) = \{\mathbf{x}\in\mathbb{R}^2\colon \inf_{\mathbf{y}\in\Omega}|\mathbf{x}-\mathbf{y}| \leq \ell\}$ the "ball" of radius ℓ around Ω.

where

$$u_{k,\mathbf{i}}(t) = \rho^k(t,\mathbf{x}_\mathbf{i}),\ \mathbf{F}_{k,\mathbf{i}} = F_k\left(\boldsymbol{\rho}(t,\mathbf{x}_\mathbf{i}), \boldsymbol{\nu}\big(\mathbf{x}_\mathbf{i}, \mathcal{I}\left[\boldsymbol{\rho}(t)\right](\mathbf{x}_\mathbf{i})\big)\right) \text{ for } k = 1,2 \text{ and } \mathbf{i} \in \mathcal{M}.$$

In order to define a numerical scheme, first we approximate the solution of (1) in a semi-discrete form by a system of ODEs

$$\frac{\mathrm{d}\boldsymbol{u}}{\mathrm{d}t} = C(\boldsymbol{u}), \tag{5}$$

where $C(\boldsymbol{u})$ is the spatial discretization of the convective term with entries given by

$$C(\boldsymbol{u}) = (C(\boldsymbol{u})_\mathbf{i})_{\mathbf{i}\in\mathcal{M}} \quad \text{with} \quad C(\boldsymbol{u})_{k,\mathbf{i}} = -\sum_{l=1}^{2} \frac{1}{h_l}\left(\hat{f}_{k,\mathbf{i}+\frac{1}{2}\mathbf{e}_l} - \hat{f}_{k,\mathbf{i}-\frac{1}{2}\mathbf{e}_l}\right),$$

for suitable numerical fluxes $\hat{f}_{k,\mathbf{i}+\frac{1}{2}\mathbf{e}_l}$ for $k,l = 1,2$ obtained by WENO reconstructions of split fluxes. For the numerical flux $f_k = \hat{f}_{k,\mathbf{i}+\frac{1}{2}\mathbf{e}_l}$, the Lax-Friedrichs-type flux splitting $f_k^{\pm}(\rho)$ is given by

$$f_k^{\pm}(\rho) = \frac{1}{2}\left(f_k(\rho) \pm \alpha_k \rho\right), \quad \alpha_k = \max_{l=1,2}\max_{\rho^k} |\partial_{\rho^k}(\rho^k(1-\rho^k))| \sup_{\mathbf{x}\in\Omega} |\nu(\mathbf{x})\cdot\mathbf{e}_l|.$$

If $\mathcal{R}^{\pm}\left(f_{k,\mathbf{i}+(-r:r)\mathbf{e}_l}\right) = \mathcal{R}^{\pm}\left(f_{k,\mathbf{i}-r\mathbf{e}_l},\ldots,f_{k,\mathbf{i}+r\mathbf{e}_l}\right)$ denotes $(2r-1)$th-order WENO upwind-biased reconstructions for $r = 2,3,4$, then

$$\hat{f}_{k,\mathbf{i}+\frac{1}{2}\mathbf{e}_l} = \mathcal{R}^{+}\left(f^{+}_{k,\mathbf{i}+(-r:r)\mathbf{e}_l}\right) + \mathcal{R}^{-}\left(f^{-}_{k,\mathbf{i}+(-r+1:r+1)\mathbf{e}_l}\right), \qquad k,l = 1,2,$$

see [10, 12]. In this work we consider third-order of accuracy in space with $r = 2$.

To evaluate the non-local terms in (1), where the convolution term $*_w$ is defined by (3), we use the following identity $\eta *_w \nabla\rho = \nabla\eta *_w \rho$, where the corresponding convolutions $\eta *_w \rho$, $(\partial\eta/\partial x_1) *_w \rho$ and $(\partial\eta/\partial x_2) *_w \rho$ are calculated approximately on the discrete grid via a quadrature formula, in our cases a composite Simpson rule. Since $\mathrm{supp}(\eta) \subset [-n_0h, n_0h]\times[-n_0h, n_0h]$ for $n_0 \in \mathbb{N}$ large enough, any convolution product is given by

$$\big(\eta * \rho(t)\big)(\mathbf{x}_\mathbf{i}) \approx \sum_{p=-n_0}^{n_0}\sum_{q=-n_0}^{n_0} h^2 c_p c_q \rho(t,\mathbf{x}_{\mathbf{i}-\mathbf{p}})\eta(\mathbf{x}_\mathbf{p}),$$

where c_p and c_q are the coefficients in the quadrature rule and $\mathbf{p} = (p,q)$. This formula for $\mathbf{u} = (u_\mathbf{i}) \in \mathbb{R}^{M\times N}$ and for the convolution product (3) can be written as

$$(\eta *_w u)(\mathbf{x}_\mathbf{i}) = \sum_{p=-n_0}^{n_0}\sum_{q=-n_0}^{n_0} h^2 c_p c_q u_{w,\mathbf{i}-\mathbf{p}}\eta(\mathbf{x}_\mathbf{p}), \tag{6}$$

where $u_{w,\mathbf{i}}$ is a discrete version of the function (4) defined by

$$u_{w,\mathbf{i}} = \begin{cases} u_{\mathbf{i}} & \text{if } \mathbf{i} \in \mathcal{M}, \\ R_w & \text{if } \mathbf{x}_{\mathbf{i}} \in B(\Omega, d(\operatorname{supp}\eta)) \setminus \Omega, \\ 0 & \text{elsewhere.} \end{cases}$$

Clearly, the discrete convolution (6) causes a computational bottleneck. This is a classical problem in scientific computing that is effectively handled by fast convolution algorithms, mainly based on Fast Fourier Transforms [13].

Finally, the semi-discrete scheme (5) is discretized by a third-order TVD Runge-Kutta time discretization method. The combined space and time discretizations define a fully discrete third-order scheme, see [3, 9] for details.

4 Numerical tests

We solve numerically (1) for $t \in [0, T]$ and $\mathbf{x} \in \Omega$ with the third-order of accuracy scheme (FD-WENO3) described in Section 3. For each iteration, the time step Δt is determinated by the formula

$$\frac{\Delta t}{h} \max\{\alpha_1, \alpha_2\} = C_{\text{cfl}}.$$

In the numerical examples we choose C_{cfl} as the largest multiple of 0.05 that yield oscillation-free numerical solutions.

In all tests, we take a classical kernel function of the form

$$\eta(\mathbf{x}) = \frac{315}{128\pi l^{18}} (l^4 - \|\mathbf{x}\|^4)^4 \chi_{[0,l]}(\|\mathbf{x}\|), \qquad \mathbf{x} \in B(\mathbf{0}, l),$$

we compare the dynamics given by different different angle amplitudes α in $\mathcal{S}(\mathbf{x}, l, \alpha, \gamma_i)$ by using conic section of the kernel given by

$$\eta_k(\mathbf{x}) = \eta(\mathbf{x}) \chi_{\mathcal{S}(\mathbf{x}, l, \alpha, \gamma_i)}(\|\mathbf{x}\|) \qquad \mathbf{x} \in B(\mathbf{0}, l) \qquad k = 1, 2.$$

Besides the circular symmetric kernel η (i.e., $\alpha = \pi$), we consider angles $\alpha \in \{\pi/2, \pi/3, \pi/6\}$. The other model parameters are set as

$$V_1 = V_2 = 4, \quad \varepsilon_1 = 0.7, \quad \varepsilon_2 = 0.3 \quad \text{and} \quad l = 0.5.$$

4.1 Example 1: bi-directional flows

We consider the evacuation problem of two populations, ρ^1 and ρ^2, moving in opposite directions in the domain $\Omega = [-4,4] \times [-1,1]$ with exits doors set at $D_1 = \{-4\} \times [-1,1]$ and $D_1 = \{4\} \times [-1,1]$ respectively. The vectors fields $\boldsymbol{\mu}^1(\mathbf{x}) = (1,0)$ and $\boldsymbol{\mu}^2(\mathbf{x}) = (-1,0)$ are fixed constantly oriented towards the right and left of the domain. Initial condition and directions of orientation in the vision field are given by

$$\begin{bmatrix} \rho_0^1 \\ \rho_0^2 \end{bmatrix}(\mathbf{x}) = \begin{bmatrix} 0.9\chi_{]-3.5,-2.5[\times]-0.5,0.5[} \\ 0.5\chi_{]2.5,3.5[\times]-0.5,0.5[} \end{bmatrix}(\mathbf{x}),$$

$$\boldsymbol{\gamma}_1(\mathbf{x}) = (1,0), \quad \boldsymbol{\gamma}_2(\mathbf{x}) = (-1,0).$$

In Figure 1, we display numerical approximations for $\rho = \rho^1 + \rho^2$, computed with $h_1 = h_2 = 1/40$ at time $T = 1.2$, for models **M1**, **M2** and **M3** with conical sections of vision with angles $\alpha \in \{\pi, \pi/2, \pi/3, \pi/6\}$. We observe that both populations scale their speed due to their own/total density and deviate from their preferred trajectory if the other group is in their view horizon. We observe the expected formation of lane patterns, which are very similar for models **M1** and **M2**, and more pronounced as the vision cone narrows. Also, model **M3** reaches higher density concentrations.

In Figure 2, we plot each population's total mass time evolution to monitor the evacuation time given by each model. We can observe that the dynamics is quite sensitive to changes in the amplitude of the vision cone. In particular, the evacuation time increases as the angle α decreases. Furthermore, we observe that model **M3** produces faster evacuation than models **M1** and **M2**.

4.2 Example 2: crossing flows

We consider two populations moving in orthogonal directions and crossing in a domain $\Omega = [-5,5] \times [-5,5]$ with exits at $x = 5$ and $y = 5$. The space available to the populations is the cross section $[-5,5] \times [-1,1] \cup [-1,1] \times [-5,5]$, due to the presences of the columns C_i, $i = 1, \ldots, 4$, described below. The vector fields, within the cross section, are fixed and oriented towards the respective exits, respectively $\{5\}\times]-1,1[$ for ρ^1 and $]-1,1[\times\{5\}$ for ρ^2. The columns, the directions of the conic section and the initial condition are given by

$$\begin{aligned} C_1 &=]-5,-1[\times]-5,-1[, \\ C_2 &=]1,5[\times]-5,-1[, \qquad & \boldsymbol{\gamma}_1(\mathbf{x}) &= (1,0), \\ C_3 &=]1,5[\times]1,5[, & \boldsymbol{\gamma}_2(\mathbf{x}) &= (0,1), \\ C_4 &=]-5,-1[\times]1,5[, \end{aligned}$$

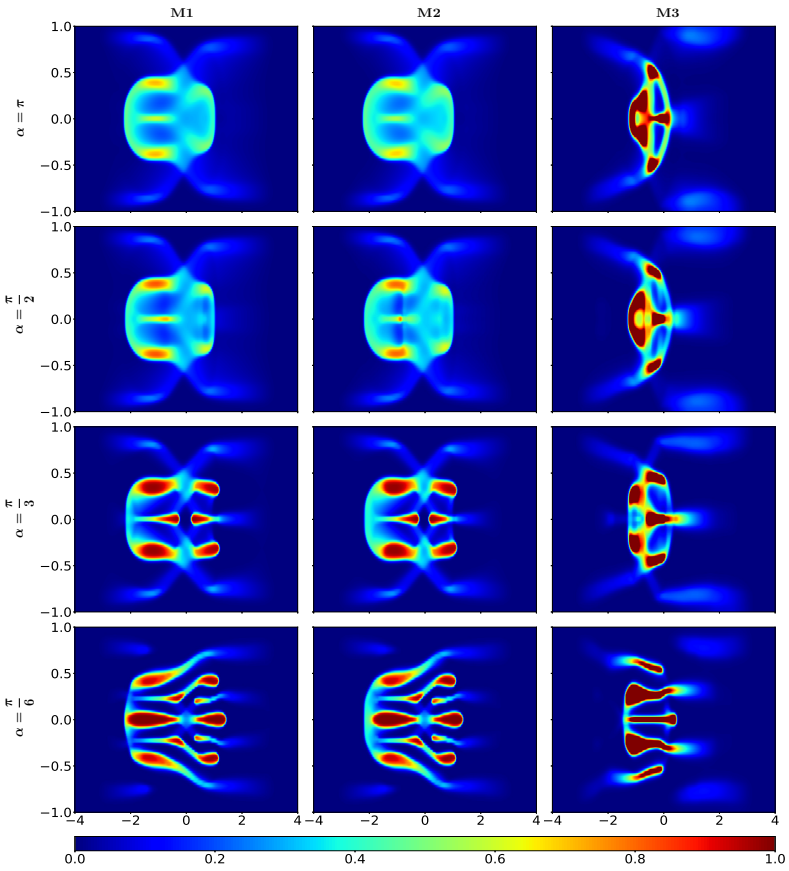

Fig. 1 Example 1: Dynamics of pedestrians flow for $\rho = \rho^1 + \rho^2$ in a bi-directional corridor at simulated time $T = 1.2$ for models **M1**, **M2** and **M3** considering different amplitudes of the cone of vision, oriented in directions $\boldsymbol{\gamma}_1 = (1, 0)$ and $\boldsymbol{\gamma}_2 = (-1, 0)$. Numerical approximations computed with FD-WENO3 with $\Delta x = \Delta y = 1/40$.

and

$$\begin{bmatrix} \rho_0^1 \\ \rho_0^2 \end{bmatrix}(\mathbf{x}) = \begin{bmatrix} 0.9\chi_{]-4.6,-3.4[\times]-0.6,0.6[} \\ 0.3\chi_{]-0.6,0.6[\times]-4.6,-3.4[} \end{bmatrix}(\mathbf{x}).$$

As in Example 1, we consider the amplitude angles $\alpha \in \{\pi, \pi/2, \pi/3, \pi/6\}$.

The numerical solutions are shown in Figure 2, with the first population ρ^1 moving to the right and the second, ρ^2, moving to the top. All the three models display a diagonal pattern orthogonal to $\boldsymbol{\gamma}_1 + \boldsymbol{\gamma}_2$, as described by various studies, see e.g. [8], which become more evident as the cone of vision reduces. As in the previous example, the behaviours of models **M1** and **M2** are similar, while **M3** displays higher density concentrations.

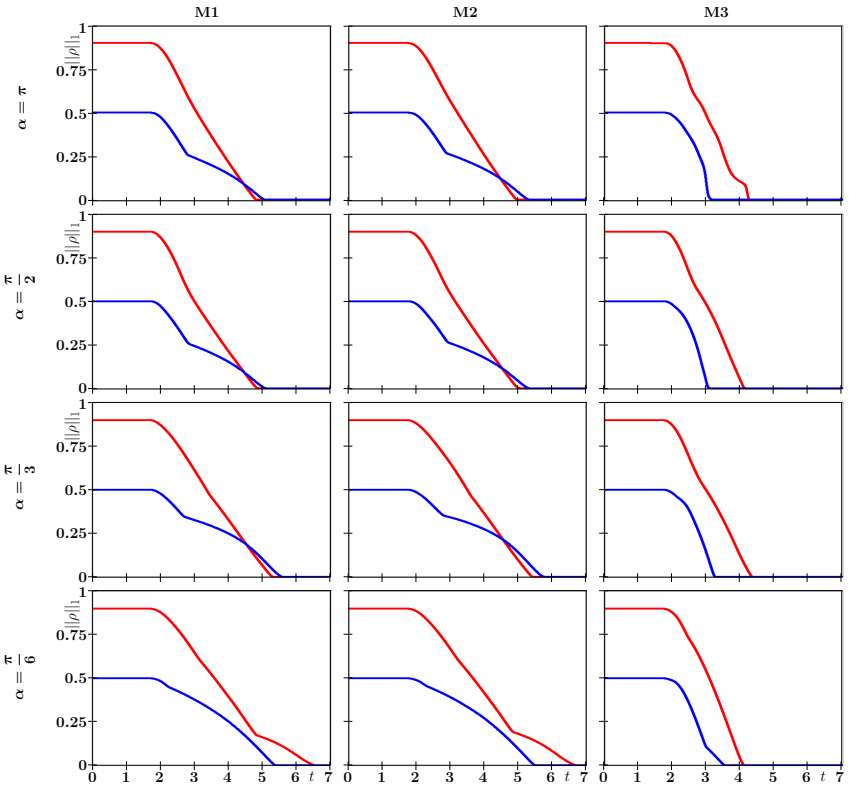

Fig. 2 Example 1: Time evolution of the total mass for ρ^1 (red) and ρ^2 (blue), and corresponding evacuation times for the models **M1**, **M2** and **M3**, with angles $\alpha = \pi$, $\pi/2$, $\pi/3$ and $\pi/6$ respectively.

5 Conclusion

In this work, we compared numerically three nonlocal macroscopic pedestrian flow models describing two populations moving in different directions. We considered anisotropic convolution kernels mimicking the effect of different cones of view to see how they affect the interaction between these populations. For the numerical simulation we used the FD-WENO3 scheme proposed in [3], obtaining the sharp pattern formation as the populations cross each other in the proposed scenarios. Furthermore, we noted that the models are very sensitive to the changes in the conic vision angles. Future work includes the simulation of more complex scenarios, and the study of the positivity preservation of the proposed high-order scheme.

Acknowledgements This work has been supported by: the French government, through the 3IA Côte d'Azur Investments in the Future project managed by the National Research Agency (ANR)

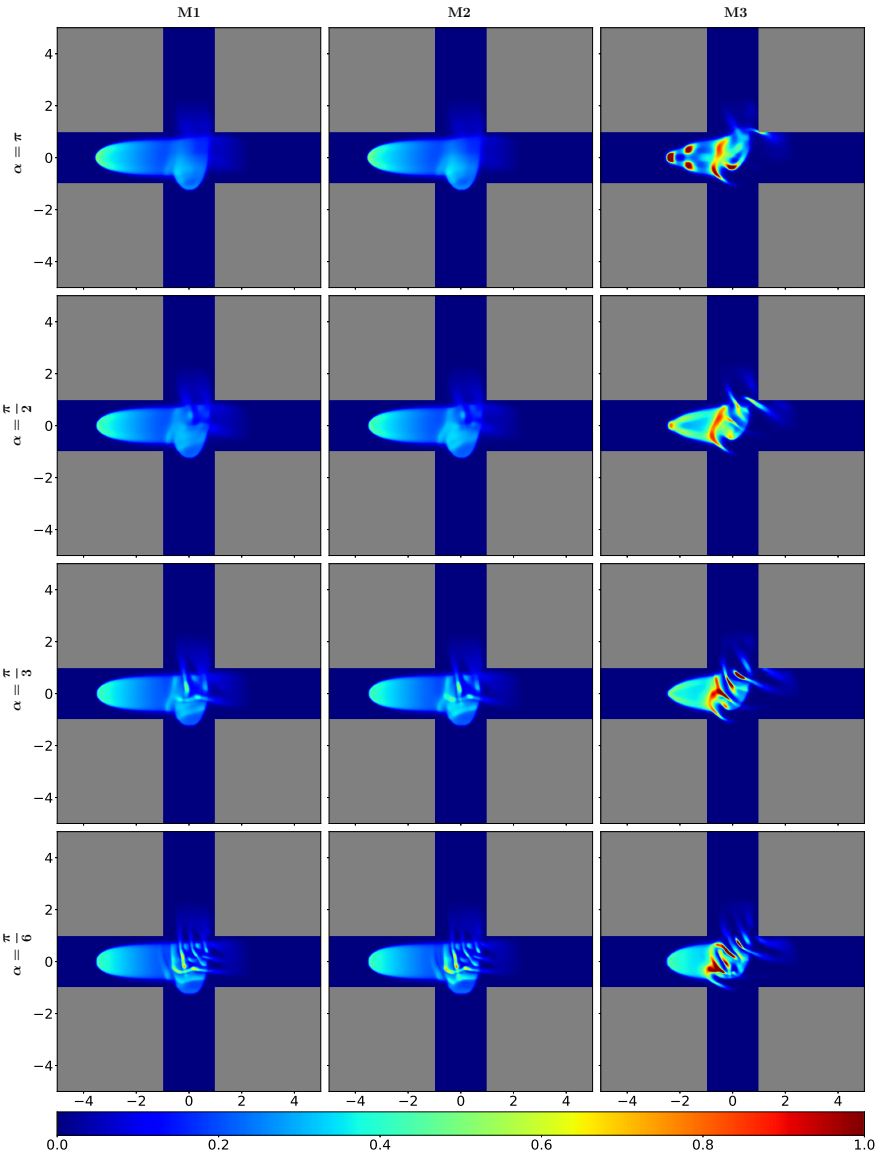

Fig. 3 Example 2: Dynamics of pedestrian flow for $\rho^1 + \rho^2$ in orthogonal crossing, at simulated time $T = 1.4$ for models **M1**, **M2** and **M3** considering different amplitudes in the angles of the vision cones oriented in directions $\boldsymbol{\gamma}_1 = (1, 0)$ and $\boldsymbol{\gamma}_2 = (0, 1)$.

with the reference number ANR-19-P3IA-0002; the Inria Associated Team “NOLOCO - Efficient numerical schemes for non-local transport phenomena” (2018-2022); the MATH-Amsud 22-MATH-05 “NOTION - NOn-local conservaTION laws for engineering, biological and epi-

demiological applications: theoretical and numerical" (2022-2023). LMV was partially supported by Centro de Modelamiento Matemático (CMM) FB210005 BASAL funds for centers of excellence from ANID-Chile.

References

1. S. Blandin and P. Goatin. Well-posedness of a conservation law with non-local flux arising in traffic flow modeling. Numer. Math., 132(2):217–241, 2016.
2. L. Bruno, A. Tosin, P. Tricerri, and F. Venuti. Non-local first-order modelling of crowd dynamics: a multidimensional framework with applications. Appl. Math. Model., 35(1):426–445, 2011.
3. R. Bürger, P. Goatin, D. Inzunza, and L. M. Villada. A non-local pedestrian flow model accounting for anisotropic interactions and domain boundaries. Math. Biosci. Eng., 17(5):5883–5906, 2020.
4. R. M. Colombo, M. Garavello, and M. Lécureux-Mercier. A class of nonlocal models for pedestrian traffic. Math. Models Methods Appl. Sci., 22(4):1150023, 34, 2012.
5. R. M. Colombo and M. Lécureux-Mercier. Nonlocal crowd dynamics models for several populations. Acta Math. Sci. Ser. B (Engl. Ed.), 32(1):177–196, 2012.
6. R. M. Colombo and E. Rossi. Nonlocal conservation laws in bounded domains. SIAM J. Math. Anal., 50(4):4041–4065, 2018.
7. R. M. Colombo and E. Rossi. Modelling crowd movements in domains with boundaries. IMA J. Appl. Math., 84(5):833–853, 2019.
8. S. P. Hoogendoorn, F. L. van Wageningen-Kessels, W. Daamen, and D. C. Duives. Continuum modelling of pedestrian flows: From microscopic principles to self-organised macroscopic phenomena. Physica A: Statistical Mechanics and its Applications, 416:684–694, 2014.
9. D. Inzunza. Métodos Implicitos-Explicitos para Problemas de Convección-Difusión-Reacción no Lineales y no Locales. PhD thesis, 2019. Universidad de Concepción.
10. G. S. Jiang and C. W. Shu. Efficient implementation of weighted ENO schemes. J. Comput. Phys., 126(1):202–228, 1996.
11. P. Kachroo, S. J. Al-Nasur, S. A. Wadoo, and A. Shende. Pedestrian Dynamics. Springer-Verlag, 2008.
12. C.-W. Shu. High order weighted essentially nonoscillatory schemes for convection dominated problems. SIAM Review, 51(1):82–126, 2009.
13. J. Von Zur Gathen and J. Gerhard. Modern Computer Algebra. Cambridge University Press, 2013.